JOURNAL OF Materials CHEMISTRY

# A study of ETS-4 molecular sieves and of their adsorption of water and ammonia

**T. Armaroli,[a] G. Busca,[a] F. Milella,[a] F. Bregani,[b] G. P. Toledo,[b] A. Nastro,[c] P. De Luca,[c] G. Bagnasco[d] and M. Turco*[d]**

[a]*Dipartimento di Ingegneria Chimica e di Processo ''G.B. Bonino'', Università, I-16129 Genova, Italy*
[b]*ENEL Ricerca, Area Generazione, 20090 Segrate (Mi), Italy*
[c]*Dipartimento di Pianificazione Trasporti ed Ambiente, Università della Calabria, Arcavacata di Rende, Cosenza, Italy*
[d]*Dipartimento di Ingegneria Chimica, Università ''Federico II'', Napoli, Italy. E-mail: turco@irc.na.cnr.it; Fax: 39-081-5936936; Tel: 39-081-7682259*

***Received 13th December 1999, Accepted 7th April 2000***
***Published on the Web 21st June 2000***

Structural and water and ammonia adsorption properties of ETS-4 were studied by means of XRD, FT-IR, Raman, UV-vis and temperature programmed desorption (TPD) techniques. XRD analysis showed that the sample was pure and highly crystalline. Skeletal IR and Raman vibrational spectra are interpreted in agreement with the structure containing chains of corner sharing $TiO_6$ octahedral zig-zag chains, tetrahedral silicate units bridging two $TiO_6$ octahedra (so giving rise to Ti–O–Si–O–Ti structures) and ''isolated'' Ti ions with an octahedral coordination involving two short bonds with oxide ions also bonded to extraframework $Na^+$ cations. Electronic spectra agree with the predominance of condensed $TiO_6$ octahedra and the absence of $TiO_2$ impurities. Two forms of molecular adsorbed water were observed from FT-IR and TPD measurements. ETS-4 adsorbed about 2 mole of water per mole of material by coordination to $Na^+$ ions. Ammonia was adsorbed in molecular form both by hydrated and anhydrous ETS-4 through hydrogen bonding with $H_2O$ molecules or coordination to $Na^+$ ions, respectively. 0.24 mole of $NH_3$ per mole ETS-4 was adsorbed in both cases.

## 1. Introduction

Zeolites are largely used industrially in the fields of chemisorption as molecular sieves and in heterogeneous catalysis technologies.[1,2] The substitution of Al for Si in a silica framework leads to a charge imbalance that must be balanced by either protons or cations in the cages. Protonic zeolites display very strong Brønsted acidity that allows these materials to have a central role in modern acid-catalyzed petrochemical processes such as fluid catalytic cracking.[3] Cation exchanged zeolites are also often utilized both in adsorption and catalysis, depending on the nature of the exchanged cation.

Recently, crystalline zeolitic silicas have been prepared, like silicalite, and their analogues, where cations other than Al have been substituted by silicon, have also been prepared and characterized.[4] Particular interest was focused on Ti silicalites,[5] which have already found industrial applications as catalysts for the hydrogen peroxide oxidation of phenol to catechol,[6] cyclohexanone plus ammonia to cyclohexanone oxime[7] and propene to propene oxide.[8] This very relevant chemistry is associated with the tetrahedral coordination of Ti substituting for silicon and, apparently, with its ability to change its overall coordination state to octahedral.[9] Ti substitution for silicon does not cause any charge imbalance, so that Ti silicalites cannot contain cations in their cages.

Recently, a new class of molecular sieve material consisting of microporous titanosilicates, named ETS (Engelhard Titanium Silicate) has received great interest for their zeolite-like properties. The so-called ETS-4, patented in 1988,[10] is a small-pore molecular sieve (*ca.* 4 Å pore diameter) whose structure was thought to be similar to that of the mineral zorite.[11] Recent studies dealt with the problem of its structure with vibrational techniques[12] and Rietveld analysis of the XRD powder.[13] In the present paper we further investigate this material from the structural point of view using XRD, skeletal FT-IR and FT-Raman spectroscopies and DR-UV-vis spectroscopy. The thermal stability and the adsorption properties of this powder are also investigated using FT-IR spectroscopy and TPD measurements.

## 2. Experimental

The synthesis system was $5.0Na_2O$–$1.2TiO_2$–$1.28HCl$–$4SiO_2$–$39.5H_2O$. The reagents used for the synthesis were in aqueous solution: NaOH (50 wt.%), $TiCl_4$ (50 wt%), HCl (36 wt%), sodium silicate ($Na_2O$ 8 wt%, $SiO_2$ 27 wt%, $H_2O$ 65 wt%). The preparation was carried out by mixing together an alkaline solution, containing sodium silicate and sodium hydroxide, with an acidic solution containing titanium tetrachloride and hydrochloric acid, without addition of seeds. The synthesis run was carried out for 24 h at $190 \pm 2$ °C under static conditions in 20 ml Teflon lined autoclaves. The reaction product was filtered, washed with distilled water and dried at 100 °C overnight. The sample was purified by ultrasound treatment in order to remove the amorphous fraction. The crystallinity of the product was determined by the method reported by Erdem and Sand.[14]

SEM micrographs of the sample were obtained by a Philips XL30 apparatus equipped with an EDAX accessory for chemical analysis. Thermal analysis (TG, DTG and DTA) was performed under constant air flow with a heating rate of 10 °C $min^{-1}$ using a Netzsch STA429 apparatus.

Specific surface areas were measured by $N_2$ adsorption at 77 K with a Carlo Erba Sorptomatic 1900.

The IR and FIR spectra were recorded by a Nicolet Magna 750 Fourier transform instrument. The skeletal spectra in the region above 400 $cm^{-1}$ were recorded with KBr pressed disks

and with a KBr beam splitter, while those in the far infrared region (400–50 $cm^{-1}$) were recorded using the powder deposited on polyethylene disks, and with a "solid substrate" beam splitter. For adsorption experiments, pressed disks of the pure powders were previously activated by outgassing at 200 °C in a conventional IR cell connected with a gas manipulation–outgassing apparatus. The FT-Raman spectra were recorded using a Bruker FTS100 (Nd–YAG laser). The Diffuse Reflectance UV-vis-NIR spectra were recorded by using a Jasco V-570 instrument.

TPD measurements were carried out in a flow apparatus. $H_2O$ thermodesorption was effected by heating the hydrated samples (0.05 g) in a He flow (30 $cm^3$ $min^{-1}$) to 600 °C at a rate of 10 °C $min^{-1}$. The concentration of $H_2O$ in the outlet of the sample cell was measured by a TCD detector. $NH_3$ thermodesorption was effected in a similar way, after saturating the sample with a 1% $NH_3$/He mixture at room temperature. A water trap (anhydrous KOH) was inserted during $NH_3$ desorption.

## 3. Results and discussion

### 3.1. XRD, DTG/DTA, SEM analysis and $N_2$ adsorption measurements

The experimental XRD pattern of ETS-4 sample is fully consistent with those reported in the patent[10] and in ref. 13.

An SEM micrograph (Fig. 1) of ETS-4 shows tetragonal laminar crystals, with uniform size of 10–15 μm and thickness of about 2 μm. A similar morphology was reported by Philippou and Anderson.[15] The Si/Ti ratio evaluated by EDAX technique was close to 2 in agreement with ref. 10.

DTG/DTA analyses show that the dehydration occurs in two steps, as reported in ref. 16. The first dehydration peak starts at room temperature and shows a maximum around 100 °C, the second one, more sharp, shows a maximum at about 290 °C. The total weight loss is 14%, corresponding to the release of about 2 moles of water per mole of ETS-4.

The crystallinity of ETS-4 was evaluated after treatments at different temperatures, by referring the intensities of the characteristic XRD peaks to those of the not heat treated material. It was found that treatment at temperatures lower than 200 °C does not affect the crystallinity of ETS-4. However the crystallinity is reduced to 72% after treatment at 200 °C and to 15% after treatment at 300 °C. The material treated at 200 °C, when exposed to moist atmosphere, readsorbs the same amount of water released during the treatment. This suggests that the molecular sieve structure is not destroyed at 200 °C but, probably, at this temperature the framework has enough energy to realize a small crystalline modification. The analysis of the XRD pattern confirms this hypothesis since the intensities of the peaks are reduced after the thermal treatment at 200 °C but the background of the pattern is not increased. A further increase of temperature up to 300 °C leads to a decrease of the XRD peaks intensity and to an increase of the background suggesting the collapse of the structure. Moreover the sample is not able to readsorb the water lost during the heat treatment. Therefore the endothermic effect observed in the DTA curve at 290 °C is due to destruction of the crystalline structure, as well as elimination of water.

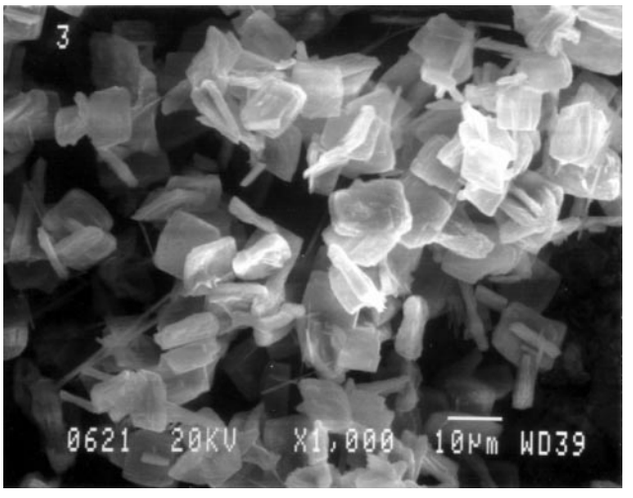


**Fig. 1** SEM micrograph of ETS-4.

Specific surface areas of ETS-4 samples hydrated and treated at 200 °C are 19 and 12 $m^2$ $g^{-1}$ respectively. Higher pretreatment temperatures were not considered because, as observed above, ETS-4 decomposes above 200 °C. The slight reduction of surface area after treatment at 200 °C indicates that this treatment, while producing a partial loss of crystallinity, does not causes a collapse of the structure, in agreement with the above results.

In Fig. 2 the corresponding $N_2$ adsorption isotherms are reported. The isotherms do not appear typical of a microporous material, notwithstanding the presence of zeolitic cages. It is very likely that the surface area values, measured by adsorption of $N_2$ at 77 K, do not take into account the whole internal surface related to zeolitic cavities, probably because the narrow pore size of this material limits the access to $N_2$ molecules at this temperature.

### 3.2. Skeletal vibrational spectra

The IR and Raman spectra of ETS-4 shown in Fig. 3 agree with those reported by Mihailova *et al.*[12] The observed IR and Raman skeletal peaks are summarized in Table 1. In addition to the skeletal bands, IR absorptions at 3585 (sharp), 3420 and 3250 $cm^{-1}$, in the O–H stretching region, and at 1650 $cm^{-1}$, typically the scissoring mode of water, can be observed. We can assign all these bands to water molecules present into the internal zeolite cavities. A weak band at 1450 $cm^{-1}$ can also be noticed.

The skeletal spectrum can be discussed in relation to the structure of zorite, as reported by Sandomirski *et al.*,[11] and the structure determined for ETS-4 by the Rietveld analysis of the XRD pattern, as reported by Cruciani *et al.*[13]

The ETS-4 structure, like any silica-based material, contains a network of silicate tetrahedra. In addition, ETS-4 and zorite structures contain zig-zag chains of corner-sharing $TiO_6$ octahedra, tetrahedral silicate units bridging two $TiO_6$ octahedra (so giving rise to Ti–O–Si–O–Ti structures). Finally, "isolated" Ti ions exist with an octahedral coordination involving two short bonds with oxide ions also bonded to

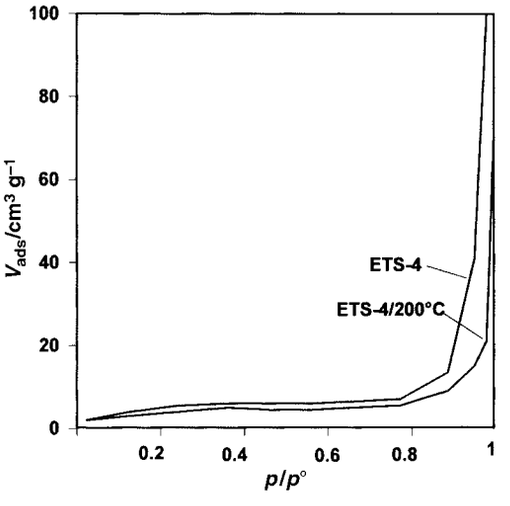


**Fig. 2** $N_2$ adsorption isotherms of ETS-4, hydrated and treated at 200 °C.

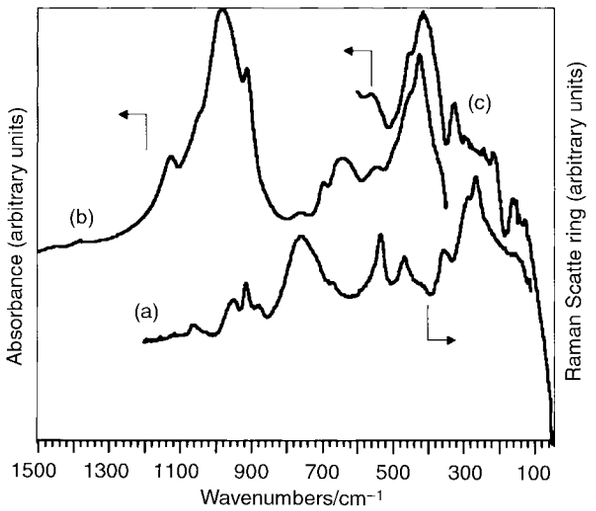


**Fig. 3** FT-Raman pure powder (a), FT-IR KBr disk (b) and FT-FIR polyethylene disk (c) spectra of ETS-4.

extraframework $Na^+$ cations. These structural units could be responsible for typical vibrational features.

**Vibrations of silica-like Si–O–Si bonds.** The vibrational modes of Si–O–Si bonds in silicas have been discussed in ref. 17.

The IR spectra of all tetrahedral silica polymorphs have bands in three regions, *i.e.* in the region 1300–950 $cm^{-1}$ (very strong, hereinafter denoted $v_1$), 850–600 $cm^{-1}$ (medium strength, $v_2$) and near 450 $cm^{-1}$ (very strong, $v_3$). Raman spectra show very weak peaks in the 1300–950 $cm^{-1}$ and 850–700 $cm^{-1}$ regions ($v_1$ and $v_2$ modes), and one or more very strong peaks below 550 $cm^{-1}$, in a position very sensitive to the overall crystal structure of the solid ($v_4$). These features are also present in the spectra of amorphous or vitreous silica; so they contain vibrations of the basic structural units of both crystalline and amorphous silica, *i.e.* $SiO_4$ tetrahedra and Si–O–Si bridging oxygens. Additional sharp peaks can be found in the IR and Raman spectra of crystalline polymorphs in the region below 700 $cm^{-1}$, and are certainly associated with splitting of the above modes, due to crystal structure effects, and with torsional lattice modes.

As for the IR spectrum, the strongest complex band, $v_1$ observed in the 1300–950 $cm^{-1}$ region, is associated with the asymmetric stretching of the Si–O–Si bridges. This mode is frequently split, due to either the in-phase ($v_1'$) or the out-of-phase coupling ($v_1''$) of the asymmetric stretching modes of the nearest Si–O–Si groups.[18] In other words, this mode somewhat couples with the symmetric and asymmetric stretching of the four Si–O bonds of the $SiO_4$ tetrahedra. The $v_1$ modes are detectable in almost the same position in the Raman spectra but are very weak there because of the small change in polarizability of Si–O–Si bonds during the asymmetric stretching.

The $v_2$ mode is essentially a bending mode of the Si–O–Si bridges, although mixed with a symmetric stretching mode, as assumed by Flanigen *et al.*.[19] It is assigned predominantly to a bending mode mainly because of its weakness in the Raman spectra, although its position is more typical of a symmetric stretching mode. This mode appears to be the least sensitive to the structure, although in some cases it splits definitely into more components.

The lowest frequency IR mode $v_3$ is associated with the out-of-plane deformation of the Si–O–Si bridges, so being a "rocking" mode. This explains why this mode is essentially silent in the Raman spectrum, while being very strong in IR in the region 430–490 $cm^{-1}$ in all silica forms as well as in zeolites.[19]

The strongest Raman mode, $v_4$, is assumed by Galeener[20] to be a symmetric stretching mode mainly because the Raman peak intensity is generally greater for stretching than for bending modes. However, the coupling of this mode with the scissoring mode, $v_2$, explains the low frequency of the strongest Raman peak (550–350 $cm^{-1}$) in all silica polymorphs. This mode is highly sensitive to the structure of the polymorph: its position, in fact, strongly depends on the type of rings present in silicas and silicates, as shown by Sharma *et al.*,[21] and on the

**Table 1** Positions ($cm^{-1}$) and assignments of the observed vibrational peaks in the IR and Raman spectra of ETS-4

| Position/$cm^{-1}$ | | Assignment | | | | |
|---|---|---|---|---|---|---|
| IR | R | $O_3$–Si–O–Si–$O_3$ | Ti–O–$SiO_3$ | (Ti–O)$_2$–$SiO_2$ | Ti–O–Ti | Na–O |
| 1127 w | | $v_{as}$ Si–O–Si | | | | |
| 1040 sh | 1062 mw | $v_1$ | | | | |
| 990 vs | | | $v_{as}$ Si–O–Ti | | | |
| 913 w | | | | $v_{as}$ Si–O–Ti | | |
| | 905 ms | | | | | |
| | 867 w | | | | $v_{as}$ Ti–O–Ti | |
| 772 | | | | | | |
| 762 w | | $\delta/v_s$ Si–O–Si | | | | |
| | | $v_2$ | | | | |
| | 742 s–br | | | | $v_s$ Ti–O–Ti | |
| 697 mw | | | | | | |
| | 657 sh | | $\delta/v_s$ Si–O–Ti | | | |
| 642 m | | | | | | |
| 545 w | | | r Si–O–Ti | | | |
| | 515 s | | | $\delta/v_s$ Si–O–Ti | | |
| | | $v_s/\delta$ Si–O–Si | | | | |
| 460 sh | | $v_4$ | | | | |
| | 446 ms | | | $\delta/v_s$ Si–O–Ti | | |
| 426 ws | | r Si–O–Si | | | | |
| | | $v_3$ | | | | |
| | 328 m | | | | $\delta$ Ti–O–Ti | |
| | 261 sh | | | | | |
| | 237 ws | | | | r Ti–O–Ti | |
| 218 | | | | | | |
| 164 | 159 | | | | | $v$ Na–O |
| | 85 vw | | | | | |

density of the unit cell, as shown by Kingma and Hemley for silicas.[22]

The weak Raman peak at 1062 $cm^{-1}$ is quite obviously assigned to Si–O–Si asymmetric stretchings $\nu_1$. The corresponding IR modes at 1123, 1040 $cm^{-1}$, evident as shoulders, and at 990 $cm^{-1}$, very strong, should also be due to Si–O–Si asymmetric stretching (IR active components). The main IR band at 426 $cm^{-1}$ is confidently assigned to the rocking of Si–O–Si bridges $\nu_3$.

**Vibrational modes involving Ti ions.** According to the structure of ETS-4, Ti–O–Ti bent bridging oxygens exist, providing three optical modes, *i.e.* an asymmetric Ti–O–Ti stretching, a symmetric stretching/in plane deformation mode, and an out of plane rocking mode. In addition, the vibrations of Ti ions must also be considered. Some of these modes should couple with the oxygen modes. From this coupling we might expect that, like for Si–O–Si modes discussed above, the Ti–O–Ti asymmetric stretching/bending mode actually splits into a very strong Raman peak mainly due to symmetric stretching, and a medium strength IR mode mainly due to in plane deformation.

Similarly, we have in the structure oxygen atoms bridging between one Ti and one Si atom. Also these oxygens provide Si–O–Ti asymmetric stretching modes, symmetric stretching/in plane deformation modes and Si–O–Ti rocking modes. In our previous study[17] we identified the Si–O–Ti asymmetric stretching of Ti silicalite (where Ti is isolated and tetrahedrally coordinated) near 960 $cm^{-1}$ with medium–strong intensity both in the IR and in the Raman spectra and we envisaged a Ti–O–Si rocking mode near 510 $cm^{-1}$ in the IR spectrum.

Medium-intensity Raman peaks and IR bands in the region 950–900 $cm^{-1}$ are usually not observed in the case of silicas. On the other hand, a quite intense Raman peak is observed in the Raman pattern of Ti silicalite just 30 $cm^{-1}$ below (*ca.* 960 $cm^{-1}$) and is due to the asymmetric stretching mode of Si–O–Ti bonds.

In agreement with this discussion, in the region 980–900 $cm^{-1}$ we expect the asymmetric stretching modes of Si–O–Ti bridges. The weak IR band at 913 $cm^{-1}$ can be assigned to the IR active components of this mode, while the split Raman peak at 938, 906 $cm^{-1}$ can be assigned to the asymmetric and symmetric components of this mode, so characterizing the Ti–O–Si–O–Ti species.

In parallel with the above assignments, the very strong Raman peak at 742 $cm^{-1}$ is likely due to the symmetric stretching of Ti–O–Ti bridges, the corresponding asymmetric stretching being probably responsible for the weak peak at 867 $cm^{-1}$.

As for the other strongest Raman modes, we propose tentatively an assignment of the peaks at 515 and 446 $cm^{-1}$ to the two expected symmetric stretching components of the Ti–O–Si–O–Ti species, while the strongest peak at 238 $cm^{-1}$ could be assigned to the rocking mode of Ti–O–Ti bridges.

The quite intense and broad IR band at 642 $cm^{-1}$ could be due to the symmetric stretching/bending mode of Si–O–Ti bridges.

### 3.3. Electronic spectra

The UV-vis spectrum of the ETS-4 sample is shown in Fig. 4. No absorption is found in the region below 30 000 $cm^{-1}$ as expected. Absorption is found in the higher wavenumber region, with the onset observed just at 30 000 $cm^{-1}$, with a first edge near 33 000 $cm^{-1}$, a shoulder at 35 000 $cm^{-1}$, a second edge near 38 000 $cm^{-1}$ and the main maximum at 40 500 $cm^{-1}$. These absorptions are certainly associated with the $O^{2-} \rightarrow Ti^{4+}$ charge transfer transition, being totally absent in the spectra of silicas, either crystalline or amorphous. We can note that bulk titanium oxides (rutile and anatase), where Ti cations take the

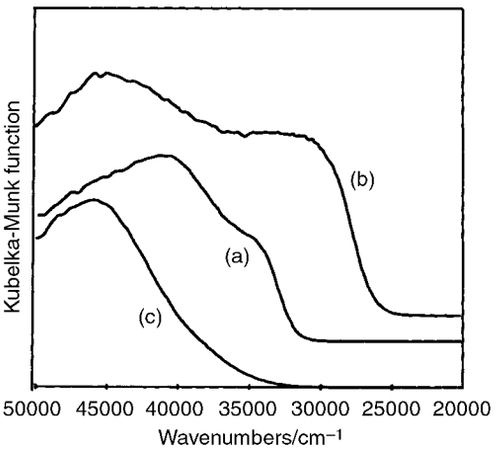


**Fig. 4** Diffuse reflectance UV-vis spectra of ETS-4 (a), anatase (b), and TS-1 (c).

octahedral coordination and share corners and edges, show an absorption edge in the region near 28 000 $cm^{-1}$ with onset near 24 000 $cm^{-1}$, as shown in Fig. 4(b). On the other hand, we found "isolated" $TiO_6$ octahedra in titania–alumina coprecipitates, characterized by a charge transfer band at 39 200 $cm^{-1}$.[23] In contrast this charge transfer transition is found as a band centered at 48 000 $cm^{-1}$ in TS1[17] and at 45 000 $cm^{-1}$ in $Ti(OC_3H_7)_4$,[24] where Ti cations are isolated and tetrahedral.

The observed edge-type absorption spectrum consequently excludes the presence of $TiO_2$ as extensive phases, and may be confidently assigned to condensed $TiO_6$ octahedra, in agreement with the proposed structure for this phase.

### 3.4 FT-IR study of the activation, adsorption and desorption of water and thermal stability

The spectra of pressed disks of the pure ETS-4 powder after outgassing at room temperature and at 200 °C are reported in Fig. 5. The strong absorption in the region 3600–2800 $cm^{-1}$ and the sharp weakly split band at 1686 (shoulder) and 1646 $cm^{-1}$, which are present after outgassing at room temperature and fully disappear after outgassing at 200 °C, are due to adsorbed molecular water (O–H asymmetric and symmetric stretchings and $H_2O$ scissoring modes). After outgassing at 200 °C a sharp weak peak at 3737 $cm^{-1}$ is detectable, together with a weak broader diffuse absorption in the region 3600–2800 $cm^{-1}$. The former small peak is certainly due to a terminal free OH group. Its sharpness and its position suggest that it is due to free silanol groups. This peak is always present as a sharp band at 3746 $\pm$ 2 $cm^{-1}$ for amorphous silicas, but was found at lower frequency, *i.e.* in the range 3738–3732 $cm^{-1}$, on silicalite, on titanium silicalite[17] and also on silicated titania.[25] This allows us to associate the small peak at

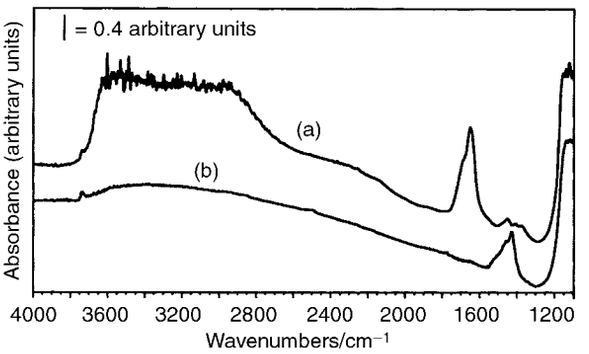


**Fig. 5** FT-IR spectra of ETS-4 pressed disk pure powder after outgassing at room temperature (a) and at 200 °C (b).

3735 $cm^{-1}$ to silanol groups associated either with structural defects and/or located at the external surface of the molecular sieve material, excluding an assignment to "extraframework" silica particles. H-bonded species, again due to structural defects, could contribute to the broad absorption in the lower frequency OH stretching region.

The spectra show a cut-off limit near 1160 $cm^{-1}$, certainly due to the higher frequency limit of the skeletal absorptions, associated with the Si–O–Si asymmetric stretching modes. However, another absorption is found, quite strong, in the spectrum of the sample outgassed at 200 °C, with a main maximum at 1426 $cm^{-1}$ and shoulders at 1458 and 1480 $cm^{-1}$. In the same region, the spectrum of the sample outgassed at room temperature presents weaker bands at 1447, 1409 and 1376 $cm^{-1}$. The change in position and growth in intensity of these bands upon outgassing at 200 °C excludes a hypothetical assignment to "bulk" vibrations, *i.e.* to overtones of the fundamental skeletal modes. This spectral region is typical for the C=O stretching modes of carbonate species, so these bands could be due to carbonate impurities formed by reaction of atmospheric $CO_2$ with the basic material.

The readsorption of water on the sample previously outgassed at 200 °C (Fig. 6) gives rise to the restoration of the sharp bands at 1643 $cm^{-1}$ (main maximum) and 1684 $cm^{-1}$ (shoulder) and of the strong absorption in the region 3600–2800 $cm^{-1}$. By further outgassing at increasing temperature it is found that the water molecules mainly desorb between 50 and 100 °C. However, after outgassing at 100 °C the shoulder at 1684 $cm^{-1}$ is fully disappeared while the main maximum at 1643 $cm^{-1}$ is still weakly present. This provides evidence for two different types of chemisorbed molecular water with a small but definite difference in their thermal stability. By repeating further these experiments we can conclude that adsorption/desorption of water is a reversible phenomenon, without any substantial change upon repeating the cycle.

As reported above ETS-4 is not a stable phase, decomposition occurs above 200 °C. We verified this by recording the spectrum of a sample treated at 400 °C. The comparison of the spectrum of the fresh sample and that after heat treatment clearly shows the complete disappearance of the IR absorptions at 3585, 3420 and 3250 $cm^{-1}$, in the O–H stretching region, and at 1650 $cm^{-1}$, certainly due to loss of water molecules and of hydroxyl groups, if any. In addition, the loss of many IR features in the skeletal region, with broadening of IR bands, seems to be an indication of an amorphization phenomenon.

### 3.5 FT-IR study of the adsorption and desorption of ammonia

Two different tests of ammonia adsorption were performed. We put into contact with ammonia vapor (100 Torr) the material simply outgassed for 3 h at room temperature and after outgassing at 200 °C for 1 h. As shown above, the first pretreatment does not allow the desorption of molecular water, so that the sample is "water covered". In the second case, instead, the sample is almost fully dehydrated.

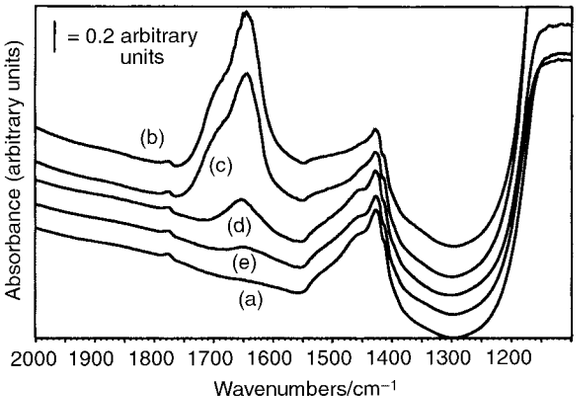


**Fig. 6** FT-IR spectra of ETS-4 pressed disk pure powder after outgassing at 200 °C (a), absorption of water and outgassing at room temperature (b), 50 °C (c), 100 °C (d) and 200 °C (e).

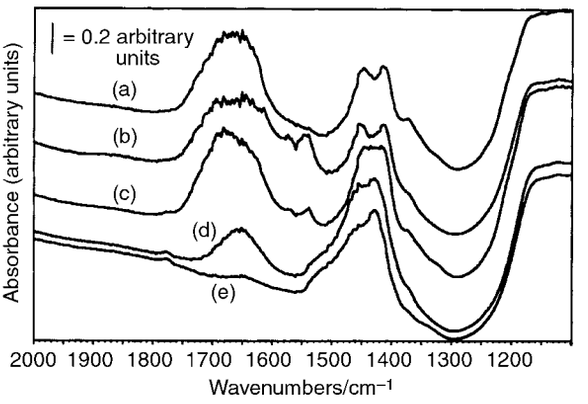


**Fig. 7** FT-IR spectra of ETS-4 pressed disk pure powder after 3 h outgassing at room temperature (a), adsorption of ammonia and outgassing at room temperature (b), 50 °C (c), 100 °C (d) and 200 °C (e).

On the "water covered sample" (Fig. 7) the adsorption of ammonia causes apparently the formation of new absorptions near 1610 $cm^{-1}$, likely due to the asymmetric deformation mode of molecular ammonia species, and near 1575 and 1543 $cm^{-1}$. The last features can be due neither to molecular ammonia nor to ammonium ions. A possible assignment is to the $NH_2$ scissoring modes of amido $NH_2$ species, typically formed by ammonia adsorption over basic oxides.[26] The analysis of the N–H stretching region does not provide any information, due to the superimposition of the bands of adsorbed water and ammonia species. Outgassing at 50 °C and 100 °C causes the progressive decrease of these features which, however, are still visible. Outgassing at 150 °C causes total desorption of ammonia but also the partial desorption of water up to total desorption of both observed at 200 °C (Fig. 6(e)). After this treatment the spectrum is the same as that obtained after outgassing of the ammonia-free original sample at the same temperature.

The adsorption of ammonia on the sample previously outgassed at 200 °C (Fig. 8 and 9) gives rise to bands near 3500, 3390, 3200 and 1640 $cm^{-1}$, due to NH stretchings and asymmetric deformation modes. This species desorbs progressively upon outgassing from 25 to 170 °C. Interestingly, the OH stretching band at 3735 $cm^{-1}$ (Fig. 6) is weakly or not affected by ammonia adsorption. On the other hand, analysis of the region just above the cutoff limit (due to the skeletal vibrations)

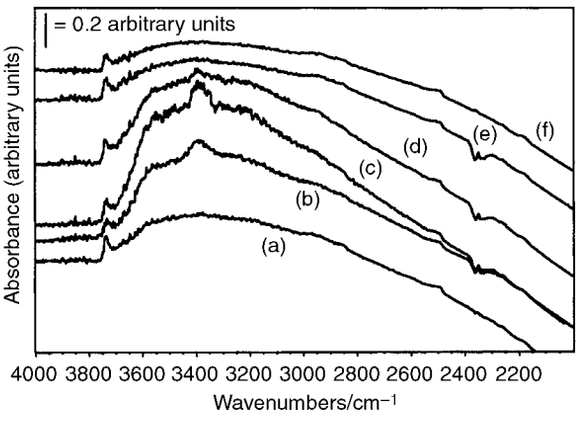


**Fig. 8** FT-IR spectra of ETS-4 pressed disk pure powder after outgassing at 200 °C (a), adsorption of ammonia and outgassing at room temperature (b), 50 °C (c), 100 °C (d), 170 °C (e) and 200 °C (f).

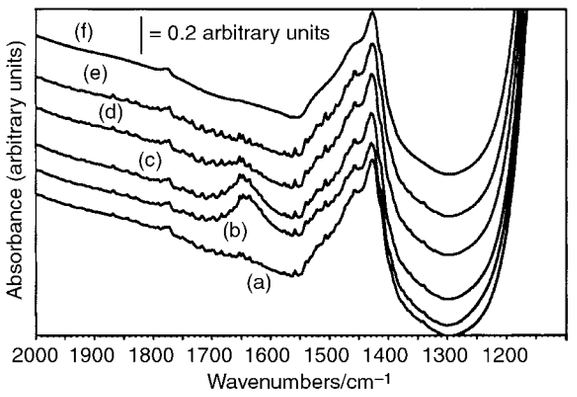


**Fig. 9** FT-IR spectra of ETS-4 pressed disk pure powder after outgassing at 200 °C (a), adsorption of ammonia and outgassing at room temperature (b), 50 °C (c), 100 °C (d), 170 °C (e) and 200 °C (f).

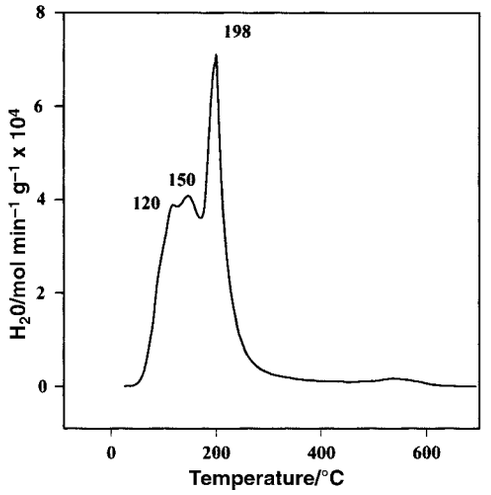


**Fig. 10** $H_2O$ TPD spectrum of ETS-4.

at 1150 $cm^{-1}$ (Fig. 8) allows us to exclude the presence of bands in this region. This indicates that the symmetric deformation mode of molecularly adsorbed ammonia species falls below this cut-off limit, so being very poorly shifted upwards with respect to the spectrum of free ammonia. This indicates that the adsorption sites for ammonia are weak Lewis sites, likely $Na^+$ cations.

### 3.6 $H_2O$ and $NH_3$ TPD studies

The $H_2O$ TPD spectrum of hydrated ETS-4 is reported in Fig. 10. It shows a composite signal with two main components with maxima at 120–150 and 198 °C. A very weak signal is also evident at high temperature (537 °C). This suggests the presence of at least two types of $H_2O$ adsorbing sites with low and medium strength leading to two forms of adsorbed water. The low and medium temperature peaks can correspond to the water outgassed in vacuum treatment at 100 and 200 °C, respectively, in FT-IR measurements. The amounts of $H_2O$ are reported in Table 2. The sodium content of ETS-4 was evaluated assuming the formula $Na_2Si_2TiO_7{\cdot}2.5H_2O$ by taking into account the observed Si/Ti ratio and hydration water content. The total amount of desorbed $H_2O$ is about 2 mol per mol of ETS-4, thus corresponding to 1 mol per mol of $Na^+$ ion. This suggests that water is coordinated to $Na^+$ ions, with a 1 : 1 stoichiometry. Since two forms of adsorbed water with different adsorption strengths are observed in the TPD spectra, the presence of $Na^+$ ions with inequivalent adsorption properties towards water can be hypothesized. This could be due to different positions, *i.e.* different coordination states of $Na^+$ ions in the ETS-4 structure. The data arising from the FT-IR and TPD studies allow us to conclude that in ETS-4 water adsorption sites are cavity $Na^+$. Both techniques suggest that at least two kinds of water molecules exist, with different vibrational spectra and thermal stability. Actually, also the XRD analysis performed by Cruciani *et al.*[13] showed the existence of different kinds of water molecules and of two different types of $Na^+$ cations in the ETS-4 cages.

$NH_3$ TPD measurements have been carried out both on hydrated ETS-4 and on the material pretreated at 200 °C. After adsorption of ammonia on the hydrated sample, the TPD spectrum (Fig. 11) shows one peak at low temperature (127 °C). It must be remarked that this temperature corresponds to the maximum temperature of the first peak in the $H_2O$ TPD spectrum (Fig. 10). This suggests that ammonia is bonded to hydration water, probably *via* a hydrogen bridge, in agreement with FT-IR results which show the presence of molecularly adsorbed ammonia and the absence of ammonium ions. However, the amount of desorbed ammonia is only 0.24 mol per mol of ETS-4, much lower than the amount of hydration water (Table 2). This is probably due to filling of pores of the sample by $H_2O$ molecules, limiting the access of $NH_3$ into the zeolitic cages of the hydrated material. On the other hand, $NH_3$

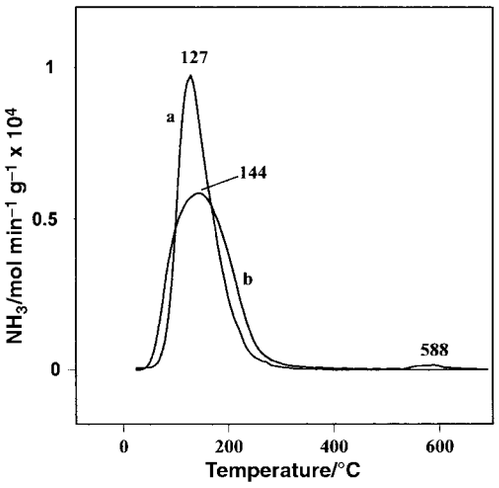


**Fig. 11** $NH_3$ TPD spectra of ETS-4: hydrated (a) and treated at 200 °C (b).

**Table 2** Water and ammonia TPD results on ETS-4

| Pretreatment temperature/°C | TPD Signal | Peak maximum temperature/°C | Desorbed amount | |
|---|---|---|---|---|
| | | | mol $g^{-1} \times 10^4$ | mol $mol^{-1}$ |
| 25 | $H_2O$ | 120 | 14.7 | 0.45 |
| | | 150 | 18.7 | 0.57 |
| | | 198 | 34.7 | 1.06 |
| | | 537 | 1.9 | 0.058 |
| 25 | $NH_3$ | 127 | 7.9 | 0.24 |
| 200 | $NH_3$ | 144 | 7.9 | 0.24 |
| | | 588 | 0.13 | 0.004 |

adsorption cannot be limited to the external surface, because the amount of adsorbed $NH_3$ corresponds to a surface concentration of $2 \times 10^{15}$ molecules $cm^{-2}$, which is larger than expected for adsorption only on the external surface. The $NH_3$ TPD spectrum of ETS-4 pretreated at 200 °C is reported in Fig. 11. A peak at rather low temperature (144 °C) is observed, besides a weak signal at high temperature (588 °C). The maximum of temperature of the main signal corresponds to the temperature range of the $NH_3$ desorption observed in FT-IR measurements. As suggested by the FT-IR results, it can be hypothesised that $NH_3$ is coordinated to $Na^+$ ions acting as Lewis acid sites. However the amount of desorbed $NH_3$, 0.24 mol per mol of ETS-4 (Table 2), is significantly lower than the $Na^+$ ions content suggesting that only a small fraction of $Na^+$ ions are able to coordinate ammonia. This could be explained supposing the existence of sterically different $Na^+$ ions with different coordination states, as discussed above. As observed for the hydrated material, the $NH_3$ TPD peak cannot be explained by only surface adsorption, because it would correspond to a concentration of adsorbing sites of $4 \times 10^{15}$ molecules $cm^{-2}$. This suggests that some penetration of ammonia into the zeolitic cages can occur. It can be hypothesised that in the hydrated and anhydrous material $NH_3$ is adsorbed on different sites: by hydrogen bonding with $H_2O$ molecules in the hydrated material or by coordination to $Na^+$ ions in the anhydrous material. However it must be observed that hydrated and anhydrous materials adsorb the same amounts of ammonia (Table 2). This behaviour could lead to an alternative hypothesis on the nature of the $NH_3$ adsorbing sites: the presence of sites specific for $NH_3$ adsorption can be supposed. These are not inhibited by the presence of $H_2O$ due to their higher affinity for $NH_3$.

The high temperature signal with very low intensity should indicate very strong $NH_3$ adsorption sites, which, however, do not belong to ETS-4, since this temperature is well beyond the stability limit of the material. These could be related to the oxides produced by the decomposition of ETS-4.

## 4 Conclusions

The results obtained in this work by employing different techniques allowed us to thoroughly characterize the structural features and adsorption properties of ETS-4. A quite complete interpretation is given for the IR and Raman skeletal spectra and for the electronic spectra of this material. These spectra fully agree with the structural properties recently given by Cruciani *et al.*[13] on the basis of the Rietveld refinement of the XRD powder pattern. The material showed significant water adsorption properties, and a lesser ability to adsorb ammonia. Adsorption sites for both molecules were identified essentially as extraframework $Na^+$ cations displaying weak Lewis acidity. Small amounts of defects giving rise to terminal silanol groups have also been evidenced by FT-IR spectroscopy. The adsorption properties were not destroyed by thermal treatment up to 200 °C. These results suggest that ETS-4 may be potentially interesting as an adsorptive material at both the gas–solid and liquid–solid interfaces. On this basis an extension of this investigation to different cationic exchanged ETS-4 is planned.

## Acknowledgements

The authors acknowledge Progetto Finalizzato MSTA II for the financial support.

## References

1 R. M. Barrer, *Zeolites and clay minerals as sorbents and molecular sieves*, Academic Press, London, 1978.
2 S. Bathia, *Zeolite Catalysts, principles and applications*, CRC Press, Boca Raton, 1990.
3 M. L. Occelli and P. O'Connor (editors), *Fluid Cracking Catalysts*, Marcel Dekker, New York, 1997.
4 R. Millini, E. Previde Massara, G. Perego and G. Bellussi, *J. Catal.*, 1992, **137**, 497.
5 B. Notari, *Adv. Catal.*, 1996, **41**, 253.
6 U. Romano, A. Esposito, F. Maspero, C. Neri and M. G. Clerici, *Chimica e Industria (Milan)*, 1990, **72**, 610.
7 P. Roffia, G. Leofanti, M. Mantegazza, M. Padovan, G. Petrini, S. Tonti and P. Gervasutti, in *New Developments in Selective Oxidation*, ed. G. Centi and F. Trifirò, Elsevier, Amsterdam, 1990, p. 43.
8 M. G. Clerici and P. Ingallina, *J. Catal.*, 1993, **140**, 71.
9 A. Zecchina, S. Bordiga, C. Lamberti, G. Ricchiardi, D. Scarano, G. Petrini, G. Leofanti and M. Mantegazza, *Catal. Today*, 1996, **32**, 97.
10 S. M. Kuznicki, *US patent* 4 938 939, 1990.
11 P. A. Sandomirski and N. Y. Belov, *Kristallografiya*, 1979, **24**, 1198.
12 B. Mihailova, V. Valtchev, S. Mintova and L. Konstantinov, *Zeolites*, 1996, **16**, 22.
13 G. Cruciani, P. DeLuca, A. Nastro and P. Pattison, *Microporous Mesoporous Mater.*, 1998, **21**, 143.
14 A. Erdem and L. B. Sand, *J. Catal.*, 1979, **60**, 241.
15 A. Philippou and W. Anderson, *Zeolites*, 1996, **16**, 98.
16 P. De Luca and A. Nastro, *Thermal characterization of ETS-4 molecular sieve*, *Proc. of Giornate Mediterranee di Calorimetria ed Analisi Termica, Chia Laguna, Cagliari*, ed. U. Sanna, PTM Editrice, Mogoro, Italy, 1998, p. 99.
17 E. Astorino, J. B. Peri, R. Willey and G. Busca, *J. Catal.*, 1995, **157**, 482.
18 E. I. Kamitsos, A. P. Patsis and E. G. Kordas, *Phys. Rev. B*, 1993, **48**, 12499.
19 E. M. Flanigen, in *Zeolites chemistry and catalysis*, ed. J. A. Rabo, American Chemical Society, Washington DC, 1979, p. 80.
20 F. L. Galeener, *Phys. Rev. B*, 1979, **19**, 4292.
21 S. K. Sharma, J. F. Mammone and M. F. Nicol, *Nature*, 1981, **292**, 140.
22 K. J. Kingma and R. J. Hemley, *Am. Mineral.*, 1994, **79**, 269.
23 A. Gutierrez- Alejandre, M. Gonzalez Cruz, M. Trombetta, G. Busca and J. Ramirez, *Microporous Mater.*, in press.
24 C. Dijkgraaf and J. P. G.-Ropusseau, *Spectrochim. Acta, Part A*, 1968, **24**, 1213.
25 L. Yi, G. Ramis, G. Busca and V. Lorenzelli, *J. Mater. Chem.*, 1994, **4**, 1755.
26 A. A. Tsyganenko, D. V. Pozdnyakov and V. N. Filimov, *J. Mol. Struct.*, 1975, **29**, 299.